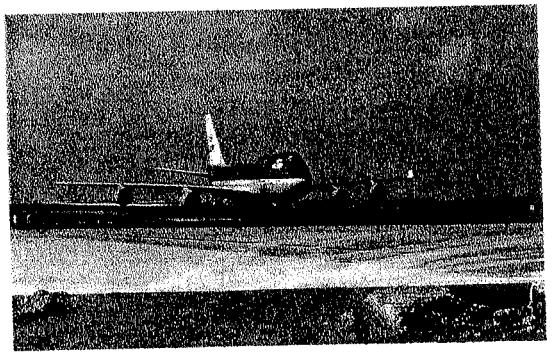

1st European Airport Pavement Workshop

11 and 12 May 2005
Dorint Sofitel Amsterdam Airport The Netherlands

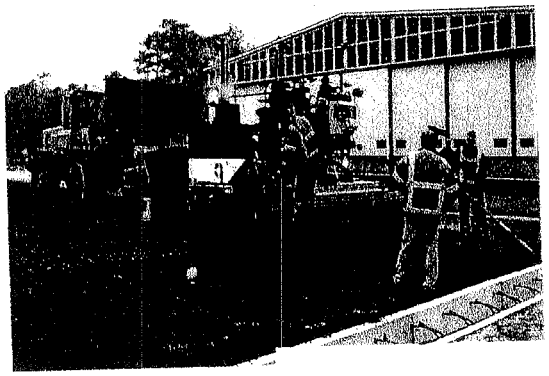

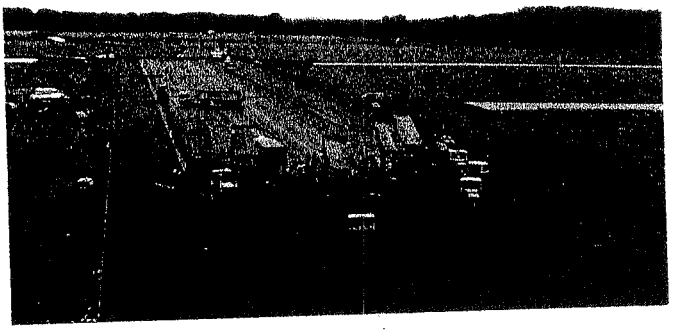

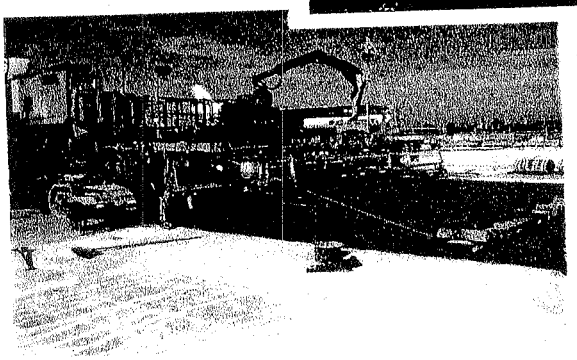

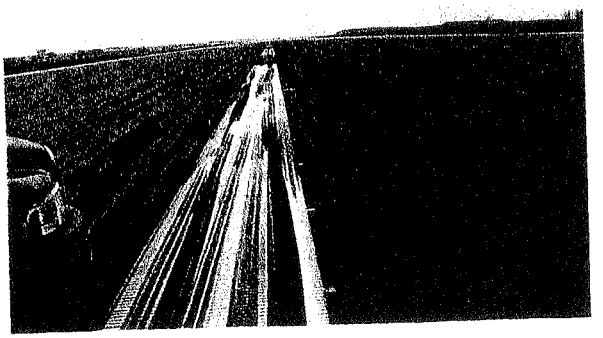

Study of Rigid Pavement Deflections Using 3-D Finite Element Analysis

Y. H. Lee, H. T. Wu, & S. T. Yen
Department of Civil Engineering, Tamkang University, Taiwan

ABSTRACT: In-depth parameter studies on the critical deflections of rigid pavements using 3-D ABAQUS finite element analysis were conducted. A systematic analytical approach was utilized to study the effects of mesh fineness and element selection. For all three loading conditions analyzed, the resulting deflections are generally in the following descending order: ABAQUS 3-D solid elements, 3-D shell elements, ILLI-SLAB element, and Westergaard solutions. Several guidelines in mesh fineness and element selection were developed and recommended.

The deflection convergence characteristics of 8-node and 9-node elements are more effective than 4-node elements. Generally speaking, with the exception of C3D8, C3D8R, and C3D27R elements, the deflections of all 3-D shell and 3-D solid elements tend to increase to convergence when a finer horizontal and or vertical mesh is used. By increasing horizontal and vertical mesh fineness, the resulting deflections of 8-node solid elements are very close to 20-node and 27-node elements. Note that the vertical mesh fineness was defined as the number of evenly divided slab layers for simplicity and practical model building concern in this study. Using vertical mesh fineness of one (or 1-layer) was proved inadequate and should be avoided for 3-D solid elements.

Based on the principles of dimensional analysis, an additional dimensionless variable (h/a) was identified and verified to have a substantial influence on ABAQUS runs using both 3-D shell and 3-D solid elements. Separate 3-D FEM deflection databases were developed using all dimensionless variables. A tentative maximum interior deflection predictive model was developed for future possible applications.

KEY WORDS: Rigid pavement, 3-D finite element analysis, deflection, convergence, backcalculation.

1. INTRODUCTION

Nondestructive deflection testing (NDT) devices have been widely adopted to obtain surface deflection data in order to evaluate existing pavement conditions using backcalculation procedures. Closed-form backcalculation procedures and graphical solutions for concrete pavements with a single slab layer (Ioannides *et al.*, 1989; Ioannides, 1990; Li *et al.*, 1996; Fwa *et al.*, 1998) are currently available. Li *et al.* (1997, 1998) further proposed a backcalculation algorithm for infinitely large rigid pavements with two slab layers through the use of an equivalent single slab layer based on the concept of equivalent flexural rigidity. Crovetti (1994) further indicated that finite slab size, the locations of loading plate (interior, edge and corner of the slab), and the presence of adjacent slabs or a tied concrete shoulder may all affect pavement surface deflections. Based on the principles of dimensional analysis, Lee *et al.* (1997, 1998) further proposed a modified deflection ratio procedure for the backcalculation of concrete pavements using various NDT devices for three different loading plate locations using 2-D FEM analysis.

Extensive re-backcalculation of general pavement study (GPS) test sections of the long term pavement performance (LTPP) program (FHWA, 1997) was not very successful. Particularly, extreme difficulties in interpreting in situ deflection measurements of rigid pavements has been encountered using multi-layered elastic backcalculation programs, probably due to the effects of temperature curling, moisture warping and loss of subgrade support. Lee and Sheu (Lee & Sheu, 2001) further investigated the effects of adjacent slabs and temperature curling on rigid pavement deflections using the plate theory approach and the two-dimensional (2-D, ILLISLAB) finite element program. Many factorial finite element runs have been carefully selected and conducted to obtain generalized deflection databases. Prediction models for deflection adjustment factors were developed to facilitate the analysis of more practical rigid pavement backcalculation problems.

With the introduction of three-dimensional (3-D, ABAQUS) FEM (Hibbitt *et al.*, 2000) and all the promising features and results reported in the literature (Kuo, 1994; Brill, 1998; Hammons, 1998; Kim & Hjelmstad, 2000; Thompson & Navneet, 1999), its applications on pavement engineering become inevitable. Nevertheless, due to the its required running-time and complexity, 3-D FEM analysis cannot be easily implemented as a part of pavement structural evaluation procedure. Thus, the main objective of this study is to conduct in-depth studies on the critical deflections of rigid pavements using 3-D FEM analysis (Wu, 2003).

2. CLOSED-FORM SOLUTIONS AND FINITE ELEMENT IDEALIZATIONS

Based on the assumption of an infinite or semi-infinite slab over a Winkler foundation, Westergaard obtained the following closed-form solutions subjected to a single edge, interior, and corner wheel load (Lee & Sheu, 2001):

$$\delta_{we} = \frac{\sqrt{2+1.2\mu}P}{\sqrt{Eh^3k}}\left[1-\frac{(0.76+0.4\mu)a}{\ell}\right]$$

$$\delta_{wi} = \frac{P}{8k\ell^2}\left\{1+\frac{1}{2\pi}\left[\ln\left(\frac{a}{2\ell}\right)-0.673\right]\left(\frac{a}{\ell}\right)^2\right\} \qquad (1)$$

$$\delta_{wc} = \frac{P}{k\ell^2}\left[1.1-0.88\left(\sqrt{2}\frac{a}{\ell}\right)\right]$$

Where δ_{we}, δ_{wi}, and δ_{wc} are the Westergaard's maximum edge, interior, and corner deflections, respectively, [L]; P is the single wheel load, [F]; h is the thickness of the slab, [L]; a is the radius of the applied load, [L]; $\ell=(E*h3/(12*(1-\mu2)*k))^{0.25}$ is the radius of relative stiffness of the slab-subgrade system [L]; k is the modulus of subgrade reaction, [FL^{-3}]; E is the concrete modulus of the slab, [FL^{-2}]; μ is the Poisson's ratio. Note that primary dimension for force is represented by [F], and length is represented by [L].

The analysis of finite slab length and width was not possible until the introduction of finite element models (FEM). The well-known ILLI-SLAB (2-D) and ABAQUS (3-D) FEM were selected for this study (Korovesis, 1990; Hibbitt *et al.*, 2000; Lee & Sheu, 2001). A brief summary of the characteristics of the ILLI-SLAB finite element, 3-D shell and solid elements from the ABAQUS library considered in this study is available (Kuo, 1994; Hammons, 1998; Wu, 2003). These include both linear and quadratic elements employing both full and reduced integration. The number of nodes, the degree of freedom, and the number of Gauss integration points per element indicating their relative complexity and required computation time are also summarized. Two types of thin shell elements (4-node, 8-node, and 9-node) are considered: those satisfy the thin shell theory (the Kirchhoff constraint) analytically and those converge to thin shell theory numerically as the thickness decreases. The selected 3-D solid (brick) elements (8-node, 20-node, and 21~27-node) include first-order (linear) and second-order (quadratic) interpolation elements. Second-order elements provide higher accuracy than first-order elements and are very effective in bending-dominated problems.

The element types S4 and S4R are general-purpose shells. The S4R5, S8R5, and S9R5 shell elements, which impose the Kirchhoff constraint numerically, are intended for the analysis of thin shells, whereas the element type S8R should be used only for thick shells. Element type C3D20 has 27 integration points, while C3D20R has only 8 integration points. The C3D27 and C3D27R elements are variable node elements, of which the number of nodes can be reduced to 21 (or any number between 21 and 27) per element by removing the interior node from each of the faces of the element as desired. Reduced integration reduces the computation time through the use of a lower-order integration to form the element stiffness. Generally speaking, the accuracy achieved with full versus reduced integration first-order elements is largely dependent on the nature of the problem. For second-order elements, reduced-integration elements generally yield more accurate results than the corresponding fully integrated elements (Hibbitt *et al.*, 2000; Hammons, 1998).

3. PARAMETER ANALYSIS AND MODEL BUILDING

A single slab resting on a Winkler foundation with three critical loading conditions was considered, though the results of interior loading will be presented in this paper primarily. To study the effects of mesh fineness and element selection on the results of FEM runs, a systematic analytical approach was utilized and implemented in a Visual Basic software package to conduct the analyzes. Several guidelines in mesh fineness and the selection of various element types are subsequently developed.

3.1 Definition of mesh fineness and mesh generation

Mesh generation in the horizontal direction generally follows the following steps: the consideration of applicable symmetry option, generation of finer mesh at the loaded area (Zone I) and at its neighborhood area (Zone II), and progressively increasing to coarser mesh further away (Zone III) for efficiency consideration. Horizontal mesh fineness is defined as

the ratio of the length of the loaded area to the selected element length throughout this study. In addition, Zone I and Zone II was chosen to have the same mesh fineness, whereas the mesh of Zone III was decided as 4 times coarser than Zone I according to previous literature. The length of neighborhood area (nC) will be further investigated, though it was usually selected as 2 times the length of the loaded area (C). Although there are some controversies regarding the mesh generation in the vertical direction (Kuo, 1994; Hammons, 1998; Ioannides, 1984), vast amount of computer resources are required if a certain aspect ratio in the vertical direction, e.g., less than 0.8, is chosen especially for a small wheel load area and/or small horizontal mesh length. Thus, it was decided that vertical mesh fineness be defined as the number of evenly divided layers for practical model building concern in this study.

3.2 Deflection convergence characteristics

A single finite slab resting on a Winkler foundation under three loading (edge, interior, corner) conditions with the following input parameters: finite slab length L=5.00m (197 in.), slab width W=5.00m (197in.), E=8.27GPa (1.2Mpsi), h=21.6cm (8.5in.), k=27MN/m^3 (100pci), tire pressure p=620kPa (90psi), μ=0.15, P=10kN (2,250lbs) was chosen for the horizontal mesh fineness study. According to the principles of dimensional analysis, this is equivalent to a pavement having a/ℓ=0.1, L/ℓ=7, W/ℓ=7, and h/a=3 to be discussed later. For higher accuracy consideration, same horizontal mesh fineness of up to 10 for Zone I and Zone II was considered, in which the length of Zone II was set to 8 times the length of the loaded area (C). The slab thickness was subdivided into up to 4 sub-layers for vertical mesh fineness study. The deflection convergence characteristics of various FEM element types were investigated. For all three loading conditions analyzed, the resulting deflections are generally in the following descending order: ABAQUS 3-D solid elements, 3-D shell elements, ILLI-SLAB element, and Westergaard solutions.

Figure 1 depicts the interior deflection convergence characteristics of 3-D shell elements. In which, deflection ratio is defined as the ratio of the resulting FEM deflections to the corresponding Westergaard solutions given in equation (1). Horizontal mesh fineness ranges from 1 to 10. The element types S8R, S8R5, and S9R5 resulted in very close deflection solutions. Generally speaking, the deflections of all 3-D shell elements tend to increase to convergence when a finer horizontal mesh is used. For 4-node shell elements, the deflections are in the following order: S4R5<S4<S4R when coarser mesh was used. The convergence characteristics of 8-node and 9-node elements are more effective than 4-node elements; and their deflections are generally slightly higher than 4-node element's deflections.

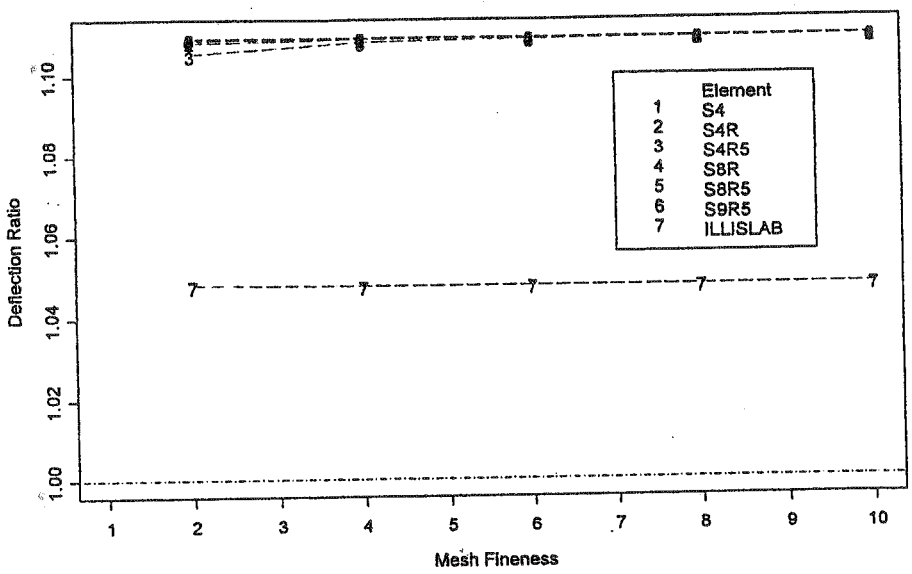

Figure 1: Interior Deflection Convergence Characteristics (3-D Shell Elements)

Figure 2 displays the interior deflection convergence characteristics of 3-D solid elements. Deflection ratio and horizontal mesh fineness are defined the same as before. The vertical mesh fineness within each plot is defined to evenly divide the slab thickness into one to four sub-layers. Using vertical mesh fineness of one (or 1-layer) was proved inadequate and should be avoided for 3-D solid elements (Wu, 2003). Especially for the C3D8R elements, the resulting deflection ratios are very different from those for the other 3-D solid elements regardless of increasing horizontal mesh fineness when vertical mesh fineness is set to one. By increasing horizontal and vertical mesh fineness, the resulting deflections of 8-node solid elements are very close to 20-node and 27-node elements. Generally speaking, the deflections of all 3-D solid elements tend to increase to convergence when a finer horizontal mesh is used. Nevertheless, the deflections of C3D20, C3D20R, and C3D27 tend to increase to convergence whereas the deflections of C3D8, C3D8R, and C3D27R tend to decrease to convergence for finer vertical mesh, i.e., sub-divided into more layers. The execution time of 20-point elements is approximate 60% of that of 27-point elements. To achieve high accuracy and computation efficiency, it was recommended that element types C3D20 or C3D27 with a horizontal mesh fineness of 3 and a vertical mesh fineness of 3 be selected for further analysis.

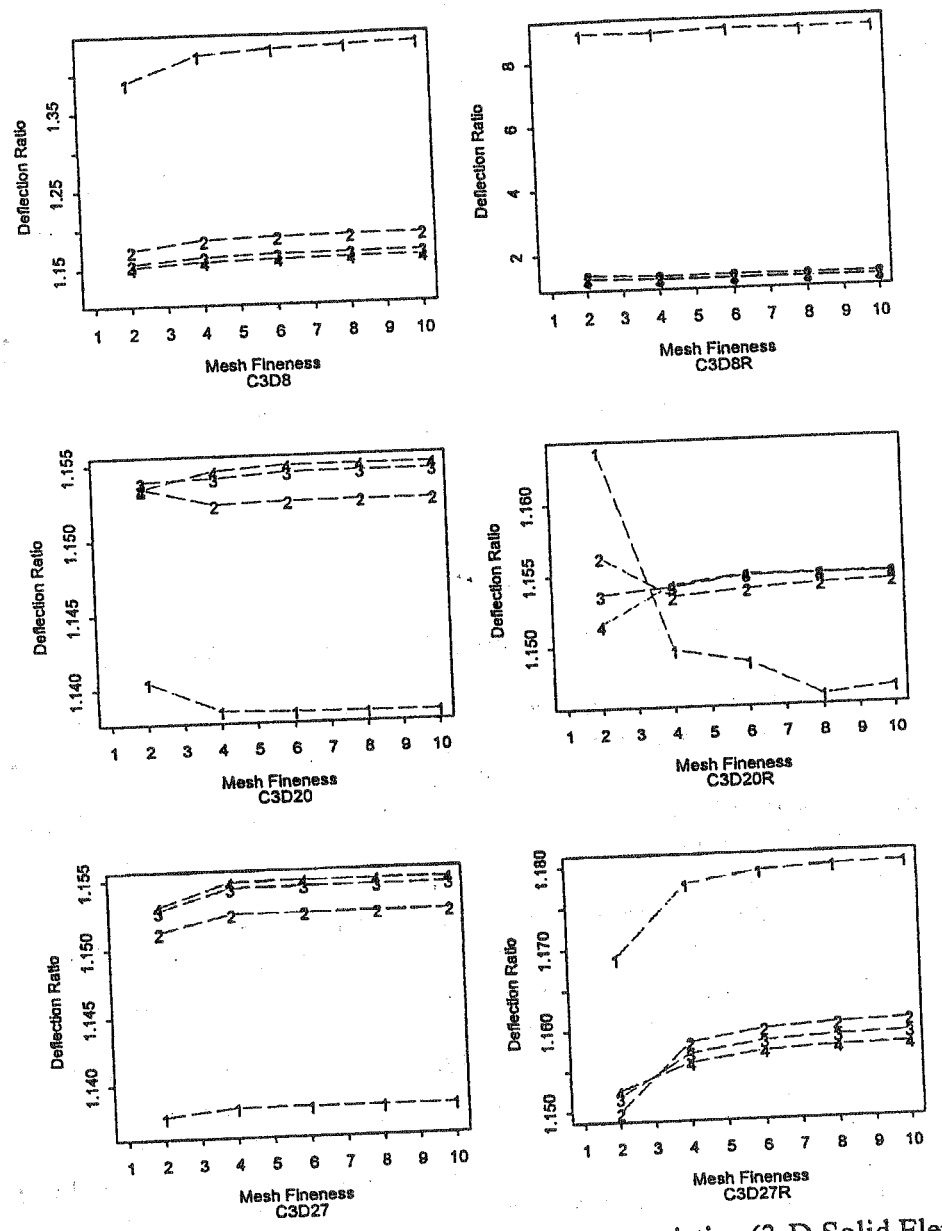

Figure 2: Interior Deflection Convergence Characteristics (3-D Solid Elements)

3.3 Convergence characteristics due to different slab thicknesses and load sizes

To investigate the effects of different slab thicknesses and load sizes to deflection convergence characteristics, a single finite slab resting on a Winkler foundation under three loading (edge, interior, corner) conditions with the following eight different sets of dominating parameters was chosen: h/α=2, 4; and a/ℓ=0.05, 0.1, 0.2, 0.3. Element type C3D27 was chosen for the remaining analyses hereafter.

The effects of horizontal mesh fineness (up to 5) to the convergence characteristics of three loading conditions were subsequently investigated, in which vertical mesh fineness was set to 3 (Wu, 2003). Similarly, the effects of vertical mesh fineness (up to 5-layer) to deflection convergence characteristics were also investigated, where horizontal mesh fineness was set to

3. Similar deflection convergence characteristics were observed. The deflections increase to convergence when finer horizontal mesh or finer vertical mesh is used for all three loading cases. The deflections of a pavement with smaller slab thickness and load size (smaller h/a and a/ℓ) converge faster.
The effect of vertical mesh fineness to deflection convergence is higher than that of horizontal mesh fineness. The thicker the pavement (larger h/a), the higher vertical mesh fineness or more layers are recommended to achieve convergence. On the other hand, simply using vertical mesh fineness of one (or 1-layer) in some earlier literature was proved to be inadequate. The recommendation of selecting a horizontal mesh fineness of 3 and a vertical mesh fineness of 3 is adequate to achieve good convergence and computation efficiency.

3.4 Determination of the length of neighborhood area

The length of neighborhood area (nC) selected for finer horizontal mesh was further investigated, in which n ranging from 1 to 8 was selected to study its effects on the results of FEM computation accuracy. The same pavement-loading system having a/ℓ=0.1, L/ℓ=7, W/ℓ=7, and h/a=3 was re-analyzed. All the aforementioned element types with a horizontal mesh fineness of 3 and a vertical mesh fineness of 3 were analyzed. The resulting deflections of any mesh fineness were compared to the corresponding ones with the finest mesh.
The deflections of ILLI-SLAB and 4-node shell elements were affected by the length of Zone II. However, the resulting deflections of 8-node and 9-node shell elements were identical when nC is greater than or equal to 2 times the length of the loaded area C. When nC is greater than or equal to 3 times C, the differences in the resulting deflection ratio of 3-D shell elements due to the selection of nC are negligible or up to 0.3%. Regardless of different nC values selected, the resulting deflection ratios of 20-node and 27-node solid elements are identical or almost identical due to the length selection of the neighborhood area and thus are not shown in separate plots for 3-D solid elements (Wu, 2003). Therefore, a value of 3 times C is recommended for all element types for consistency and conservative consideration.

4. IDENTIFICATION OF ADDITIONAL DIMENSIONLESS VARIABLE

According to Ioannides & Salsilli-Murua (1989), the following relationship has been identified and verified through many 2-D FEM studies for a constant Poisson's ratio:

$$\frac{\delta k \ell^2}{P} = f\left(\frac{a}{\ell}, \frac{L}{\ell}, \frac{W}{\ell}\right) \tag{2}$$

Extreme difficulties were encountered while using only these three dimensionless variables for 3-D FEM analyses. Based on the principles of dimensional analysis, in addition to the normalized load radius (a/ℓ), the normalized finite slab length (L/ℓ), and the normalized finite slab width (W/ℓ), an additional dominating dimensionless variable (h/a) defined as the ratio of slab thickness (h) and load radius (a) was subsequently identified. The following relationship can account for the theoretical differences of various 3-D shell and 3-D solid elements:

$$\frac{\delta k \ell^2}{P} = f\left(\frac{a}{\ell}, \frac{L}{\ell}, \frac{W}{\ell}, \frac{h}{a}\right) \tag{3}$$

This relationship was numerically verified with a series of factorial runs using the selected element type C3D27 and all the 3-D shell elements under three loading cases (interior, edge,

and corner). While keeping the above four dimensionless variables constant and changing any other input parameters (a, h, ℓ, L, W, E, k, P), the resulting dimensionless 3-D FEM deflections ($\delta k\ell^2/P$) remained constant. Some results for interior loading analysis with excellent agreements are summarized in Table 1 and Table 2.

5. DEVELOPMENT OF DATABASES AND PREDICTION MODELS

An automated analysis program was developed using the Visual Basic software package (Microsoft, 1998) to automatically construct FEM models, generate the input files, conduct the runs, as well as summarize the results. This program was also capable of assisting in conducting all the aforementioned analyses through the selection of different loading locations, various 3-D shell and solid elements, horizontal and vertical mesh fineness, and the length of the Zone II.

A series of 3-D FEM factorial runs was conducted for a single slab resting on a Winkler foundation with three critical loading conditions based on the following dimensionless parameters: L/ℓ=2~7 (step by 1); W/ℓ=2, 3, 4, 5, 6, 7 (step by 1); a/ℓ=0.05, 0.1~0.5 (step by 0.1); and h/a=0.5~6 (step by 0.5). These ranges were carefully selected to cover a very wide range of highway and airfield rigid pavement conditions. Separate deflection databases were created using element type C3D27 with a horizontal mesh fineness of 3, a vertical mesh fineness of 3, and the same finer mesh extended to 3 times the length of loaded area (C). Since the resulting deflection ratios defined as the ratio of 3-D FEM results to Westergaard solutions always have a value greater than one, the reciprocal of the deflection ratios (R) or adjustment factor ranges from 0 to 1 will satisfy the following concise relationship:

$$R = \frac{1}{\text{Deflection Ratio}} = \frac{\delta_w}{\delta_{3D}} = f\left(\frac{a}{\ell}, \frac{L}{\ell}, \frac{W}{\ell}, \frac{h}{a}\right) \tag{4}$$

In which, δ_w and δ_{3D} represent the Westergaard deflections and 3-D FEM deflections, [L]. The 3-D FEM deflections are always higher than the Westergaard solutions. The very high deflection ratios (or very small Rs) occurred when a thicker pavement (larger h/a) or a larger load size (larger a/ℓ) was analyzed. Since Westergaard's deflection is very small for thicker pavements or larger load sizes (larger h/a and a/ℓ), the resulting 3-D FEM deflections can be several times of the theoretical solutions due to possible compression across the slab thickness.

Table 1: Identification of Dimensionless Variables (Interior Loading, C3D27 Element)

h/a	a/ℓ	L/ℓ	W/ℓ	C	a	h	ℓ	L	W	E	k	p	P	σ	δ	σh^2/P	δ*kℓ^2/P
				cm	cm	cm	cm	m	m	GPa	MN/m^3	kPa	kN	kPa	mm		
1.5	0.2	2	2	12.7	7.2	10.7	35.8	0.72	0.72	13.78	88.1	482.3	7.8	751.7	0.1924	1.1160	0.2811
1.5	0.2	2	2	19.1	10.7	16.1	53.7	1.07	1.07	10.34	44.1	620.1	22.5	966.0	0.4947	1.1156	0.2810
1.5	0.2	2	2	19.1	10.7	16.1	53.7	1.07	1.07	13.78	58.7	551.2	20.0	858.5	0.3298	1.1154	0.2810
1.5	0.2	2	2	25.4	14.3	21.5	71.7	1.43	1.43	24.12	77.1	689.0	44.5	1073.5	0.3141	1.1159	0.2810
1.5	0.2	2	2	25.4	14.3	21.5	71.7	1.43	1.43	31.01	99.1	1033.5	66.8	1610.2	0.3665	1.1159	0.2810
1.5	0.2	2	2	31.8	17.9	26.9	89.6	1.79	1.79	20.67	52.9	895.7	90.4	1395.2	0.5955	1.1157	0.2810
1.5	0.2	2	2	31.8	17.9	26.9	89.6	1.79	1.79	27.56	70.5	413.4	41.7	644.1	0.2061	1.1159	0.2810
1.5	0.2	2	2	38.1	21.5	32.2	107.5	2.15	2.15	13.78	29.4	826.8	120.2	1288.4	0.9894	1.1160	0.2810
1.5	0.2	2	2	38.1	21.5	32.2	107.5	2.15	2.15	41.34	88.1	620.1	90.1	966.0	0.2474	1.1156	0.2810
1.5	0.2	2	2	38.1	21.5	32.2	107.5	2.15	2.15	27.56	58.7	689.0	100.1	1073.5	0.4123	1.1158	0.2810
1.5	0.2	2	2	38.1	21.5	32.2	107.5	2.15	2.15	13.78	5639.9	482.3	7.8	37.1	0.0056	0.8811	0.5256
6.0	0.2	4	4	12.7	7.2	43.0	35.8	1.43	1.43	10.34	2820.0	620.1	22.5	47.7	0.0145	0.8812	0.5256
6.0	0.2	4	4	19.1	10.7	64.5	53.7	2.15	2.15	13.78	3760.0	551.2	20.0	42.4	0.0096	0.8812	0.5256
6.0	0.2	4	4	19.1	10.7	64.5	53.7	2.15	2.15	24.12	4934.9	689.0	44.5	53.0	0.0092	0.8810	0.5256
6.0	0.2	4	4	25.4	14.3	86.0	71.7	2.87	2.87	31.01	6344.9	1033.5	66.8	79.4	0.0107	0.8808	0.5256
6.0	0.2	4	4	25.4	14.3	86.0	71.7	2.87	2.87	20.67	3384.0	895.7	90.4	68.9	0.0174	0.8811	0.5256
6.0	0.2	4	4	31.8	17.9	107.5	89.6	3.58	3.58	27.56	4512.0	413.4	41.7	31.8	0.0060	0.8812	0.5256
6.0	0.2	4	4	31.8	17.9	107.5	89.6	3.58	3.58	13.78	1880.0	826.8	120.2	63.6	0.0289	0.8809	0.5256
6.0	0.2	4	4	38.1	21.5	129.0	107.5	4.30	4.30	41.34	5639.9	620.1	90.1	47.7	0.0072	0.8810	0.5256
6.0	0.2	4	4	38.1	21.5	129.0	107.5	4.30	4.30	27.56	3760.0	689.0	100.1	53.0	0.0120	0.8810	0.5256

Table 2: Identification of Dimensionless Variables (Interior Loading, 3-D Shell Elements)

Number	h/a	a/ℓ	L/ℓ	W/ℓ	C	a	h	ℓ	L	W	E	k	p	P
					cm	cm	cm	cm	m	m	GPa	MN/m^3	kPa	kN
1	6.0	0.1	5	5	25.4	14.33	85.98	143.3	3.58	3.58	3.1666	40.5	620.1	40.05
2	6.0	0.1	5	5	50.8	28.66	171.97	286.6	7.17	7.17	8.4471	54.0	620.1	160.20
3	6.0	0.1	5	5	25.4	14.33	85.98	143.3	3.58	3.58	8.4471	108.0	620.1	40.05
4	4.0	0.1	5	5	12.7	7.17	28.66	71.7	1.79	1.79	17.8107	135.0	620.1	10.01
5	4.0	0.1	5	5	12.7	7.17	28.66	71.7	1.79	1.79	14.2485	108.0	620.1	10.01
6	4.0	0.1	5	5	25.4	14.33	57.32	143.3	3.58	3.58	42.7456	162.0	620.1	40.05
7	0.5	0.1	5	5	12.7	7.17	3.58	71.7	1.79	1.79	2736.0190	40.5	620.1	10.01
8	0.5	0.1	5	5	12.7	7.17	3.58	71.7	1.79	1.79	2736.0190	40.5	620.1	10.01
9	0.5	0.1	5	5	25.4	14.33	7.17	143.3	3.58	3.58	25534.3400	189.0	620.1	40.05
10	6.0	0.4	5	5	38.1	21.50	128.97	53.7	1.34	1.34	0.0186	40.5	620.1	90.11
11	6.0	0.4	5	5	10.2	5.73	34.39	14.3	0.36	0.36	0.0049	40.5	620.1	6.41
12	6.0	0.4	5	5	7.6	4.30	25.79	10.7	0.27	0.27	0.0223	243.0	620.1	3.60
13	4.0	0.4	5	5	25.4	14.33	57.32	35.8	0.90	0.90	0.2226	216.0	620.1	40.05
14	4.0	0.4	5	5	20.3	11.47	45.86	28.7	0.72	0.72	0.0334	40.5	620.1	25.63
15	4.0	0.4	5	5	22.9	12.90	51.59	32.2	0.81	0.81	0.0376	40.5	620.1	32.44
16	0.5	0.4	5	5	25.4	14.33	7.17	35.8	0.90	0.90	28.4970	54.0	620.1	40.05
17	0.5	0.4	5	5	22.9	12.90	6.45	32.2	0.81	0.81	19.2369	40.5	620.1	32.44
18	0.5	0.4	5	5	25.4	14.33	7.17	35.8	0.90	0.90	21.3728	40.5	620.1	40.05

Number	RPB12		S4		S4R		S4R5		S8R		S8R5		S9R5	
	Delection (mm)	δkℓ^2/P	Delection (mm)	δkℓ^2/P	Delection (mm)	δkℓ^2/P	Delection (mm)	δkℓ^2/P	Delection (mm)	δkℓ^2/P	Delection (mm)	δkℓ^2/P	Delection (mm)	δkℓ^2/P
1	0.0660	0.1378	0.0826	0.1726	0.0826	0.1726	0.0824	0.1721	0.0826	0.1725	0.0826	0.1725	0.0826	0.1725
2	0.0495	0.1378	0.0620	0.1726	0.0620	0.1726	0.0618	0.1721	0.0619	0.1725	0.0619	0.1725	0.0619	0.1725
3	0.0247	0.1378	0.0310	0.1726	0.0310	0.1726	0.0309	0.1721	0.0310	0.1725	0.0310	0.1725	0.0310	0.1725
4	0.0198	0.1378	0.0220	0.1533	0.0220	0.1533	0.0220	0.1531	0.0220	0.1534	0.0220	0.1534	0.0220	0.1534
5	0.0247	0.1378	0.0275	0.1533	0.0275	0.1533	0.0275	0.1531	0.0275	0.1534	0.0275	0.1534	0.0275	0.1534
6	0.0165	0.1377	0.0184	0.1533	0.0184	0.1534	0.0183	0.1531	0.0184	0.1534	0.0184	0.1534	0.0184	0.1534
7	0.0660	0.1378	0.0661	0.1380	0.0661	0.1380	0.0661	0.1380	0.0661	0.1381	0.0661	0.1381	0.0661	0.1381
8	0.0660	0.1378	0.0661	0.1380	0.0661	0.1380	0.0661	0.1380	0.0661	0.1381	0.0661	0.1381	0.0661	0.1381
9	0.0141	0.1379	0.0141	0.1379	0.0142	0.1380	0.0142	0.1380	0.0142	0.1381	0.0142	0.1381	0.0142	0.1381
10	1.0035	0.1310	2.6899	0.3511	2.6899	0.3511	2.6518	0.3462	2.6670	0.3481	2.6670	0.3481	2.6670	0.3481
11	1.0035	0.1310	2.6899	0.3511	2.6899	0.3511	2.6518	0.3462	2.6670	0.3482	2.6670	0.3482	2.6670	0.3482
12	0.1673	0.1310	0.4484	0.3512	0.4485	0.3512	0.4419	0.3461	0.4445	0.3481	0.4445	0.3481	0.4445	0.3481
13	0.1882	0.1310	0.3427	0.2386	0.3428	0.2387	0.3392	0.2362	0.3411	0.2375	0.3411	0.2375	0.3411	0.2375
14	1.0035	0.1310	1.8278	0.2386	1.8284	0.2387	1.8089	0.2361	1.8190	0.2375	1.8191	0.2375	1.8191	0.2375
15	1.0035	0.1310	1.8277	0.2386	1.8284	0.2387	1.8089	0.2361	1.8190	0.2374	1.8191	0.2375	1.8191	0.2375
16	0.7526	0.1310	0.7601	0.1323	0.7607	0.1324	0.7603	0.1323	0.7628	0.1328	0.7627	0.1328	0.7627	0.1328
17	1.0034	0.1310	1.0135	0.1323	1.0142	0.1324	1.0136	0.1323	1.0170	0.1328	1.0169	0.1327	1.0169	0.1327
18	1.0035	0.1310	1.0135	0.1323	1.0143	0.1324	1.0137	0.1323	1.0171	0.1328	1.0170	0.1328	1.0170	0.1328

To facilitate the future possible applications of these databases, the following predictive model was developed for maximum interior deflection estimation using projection pursuit regression technique (Lee & Darter, 1994; Friedman & Stuetzle, 1981):

$$R = 0.57628 + 0.29988\ \Phi_1 + 0.03984\,\Phi_2$$

$$\Phi_1 = \begin{cases} 1.15062 + 3.59112(A1) + 1.41207(A1)^2 + 0.16542(A1)^3 & \text{if } (A1) \le 0 \\ 1.00125 + 1.81296(A1) - 2.35892(A1)^2 - 6.28127(A1)^3 & \text{if } (A1) > 0 \end{cases}$$

$$\Phi_2 = \begin{cases} -14.76436 + 25.89010(A2) - 13.77861(A2)^2 + 2.28462(A2)^3 & \text{if } (A2) \le 2 \\ 9.85184 - 9.96245(A2) + 3.28991(A2)^2 - 0.36233(A2)^3 & \text{if } (A2) > 2 \end{cases} \quad (5)$$

$$A1 = 0.57228x1 + 0.02624x2 - 0.02631x3 - 0.81921x4$$

$$A2 = -0.64426x1 + 0.18742x2 + 0.04724x3 + 0.73998x4$$

$$X = [x1, x2, x3, x4] = \left[\frac{a}{\ell}, \frac{L}{\ell}, \frac{h}{a}, \frac{h}{a} * \frac{a}{\ell}\right]$$

$$\textit{Limits}: 0.05 \le a/\ell \le 0.5, 0.5 \le h/a \le 6.0, 3 \le L/\ell \le 8, W/\ell = L/\ell$$

Statistics : $N = 432, R^2 = 0.9954, SEE = 0.02022$

In which, N stands for the number of observations; R^2 is the coefficient of determination; SEE is the standard error of the estimation. Note that the effect of finite slab width is similar to that of finite slab length. For simplification, the finite slab width is set to equal to the finite slab length and thus is excluded from this analysis.

6. CONCLUSIONS AND RECOMMENDATIONS

In-depth parameter studies on the critical deflections of rigid pavements using 3-D ABAQUS finite element analysis were conducted. A systematic analytical approach was utilized and implemented in a Visual Basic software package to automatically conduct the analyses for consistency and efficiency consideration. For all three loading conditions analyzed, the resulting deflections are generally in the following descending order: ABAQUS 3-D solid elements, 3-D shell elements, ILLI-SLAB element, and Westergaard solutions.

The deflection convergence characteristics of 8-node and 9-node elements are more effective than 4-node elements. Generally speaking, with the exception of C3D8, C3D8R, and C3D27R elements, the deflections of all 3-D shell and solid elements tend to increase to convergence when a finer horizontal and or vertical mesh is used. By increasing horizontal and vertical mesh fineness, the resulting deflections of 8-node solid elements are very close to 20-node and 27-node elements. Using vertical mesh fineness of one (or 1-layer) was proved inadequate and should be avoided for 3-D solid elements. Especially for the C3D8R elements, the resulting deflection ratios are very different from those for the other 3-D solid elements regardless of increasing horizontal mesh fineness when vertical mesh fineness is set to one. The vertical mesh fineness was defined as the number of evenly divided slab layers for simplicity and practical model building concern in this study. To achieve high accuracy and computation efficiency, the selection of element types C3D20 or C3D27 with a horizontal mesh fineness of 3 and a vertical mesh fineness of 3 may be adequate.

Similar conclusions were reached for mesh fineness and element selection study using different slab thicknesses (h/a) and load sizes (a/ℓ). The deflections of ILLI-SLAB and 4-node elements were affected by the length of neighborhood area (Zone II) whereas the differences in deflections due to the selection of nC are limited or negligible for 3-D shell and 3-D solid elements. Thus, a value of 3 times C was recommended for all element types for consistency and conservative consideration.

An additional dominating dimensionless variable (h/a) defined as the ratio of slab thickness (h) and load radius (a) was identified and verified to have a substantial influence on ABAQUS runs using both 3-D shell and 3-D solid elements. Together with the normalized load radius (a/ℓ), the normalized finite slab length (L/ℓ), and the normalized finite slab width (W/ℓ), this additional mechanistic variable can be used to account for the differences among various 2-D, 3-D FEM idealizations, and theoretical closed-form deflection solutions. Separate deflection databases were created using these four variables for C3D27 element. An example maximum interior deflection predictive model in terms of adjustment factors (ranging from 0 to 1) was presented for future possible applications. The ultimate goal is to bridge the gap among various 2-D and 3-D FEM idealizations and closed-form solutions for future development of a backcalculation procedure based on the results of 3-D FEM analysis (Lee *et al.*, 1997; 1998; Lee & Sheu, 2001; Wu, 2003).

REFERENCES

Brill, D. R. (1998). *Development of Advanced Computational Models for Airport Pavement Design*. DOT/FAA/AR-97/47.

Crovetti, J. A. (1994). *Design and evaluation of jointed concrete pavement systems incorporating free draining base layers*. Ph.D. dissertation, Univ. of Illinois, Urbana.

FHWA (1997). *Backcalculation of layer moduli of LTPP general pavement study (GPS) sites. Res. Rep. FHWA-RD-97-086.*, FHWA, Washington, D.C.

Friedman, J. H. and W. Stuetzle (1981). "Projection Pursuit Regression," *Journal of the American Statistical Association*, Vol. 76, pp. 817-823.

Fwa, T. F., Tan, K. H., and Li, S. (1998). "Graphical solutions for back-calculation of rigid pavement parameters." *J. of Transp. Engrg., ASCE, 124(1)*, 102-104.

Hammons, M. I. (1998). *Advanced Pavement Design: Finite Element Modeling for Rigid Pavement Joints*. Report II: Model Development, DOT/FAA/AR-97-7.

Hibbitt, Karlsson, and Sorensen (2000). ABAQUS/Standard User's Manual. Vol. I & II.

Ioannides, A. M. (1984). *Analysis of Slabs-on-Grade for a Variety of Loading and Support Conditions*. Ph.D. Dissertation, University of Illinois, Urbana, Illinois.

Ioannides, A. M. (1990). "Dimensional analysis in NDT rigid pavement evaluation." *J. Transp. Engrg., ASCE, 116(1)*, 23-36.

Ioannides, A. M., Barenberg, E. J., and Lary, J. A. (1989). "Interpretation of falling weight deflectometer results using principles of dimensional analysis." *Proc., 4th Int. Conf. on concrete pavement design and rehabilitation*, Purdue University, West Lafayette, Indiana, 231-247.

Ioannides, A. M. and R. A. Salsilli-Murua (1989). "Temperature Curling in Rigid Pavements: An Application of Dimensional Analysis." In *Transportation Research Record* 1227, pp. 1-11.

Kim., J., and K. Hjelmstad (2000). *Three-Dimensional Finite Element Analysis of Multi-Layered Systems: Comprehensive Nonlinear Analysis of Rigid Airport Pavement Systems*, Federal Aviation Administration DOT 95-C-001.

Korovesis, G. T. (1990). *Analysis of Slab-on-Grade Pavement Systems Subjected to Wheel and Temperature Loadings*. Ph.D. Dissertation, University of Illinois, Urbana, Illinois.

Kuo, C. M. (1994). *Three-Dimensional Finite Element Model for Analysis of Concrete Pavement Support*. Ph.D. Dissertation, University of Illinois, Urbana, Illinois.

Lee, Y. H. (1993). *Development of Pavement Prediction Models*. Ph.D. Dissertation, University of Illinois, Urbana, Illinois.

Lee, Y. H. (1999). "TKUPAV: Stress Analysis and Thickness Design Program for Rigid Pavements," *J. of Transp. Engrg., ASCE,*, Vol. 125, No. 4, pp. 338-346.

Lee, Y. H., Lee, C. T., and Bair, J. H. (1997). *Development of a backcalculation program for jointed concrete pavements. Res. Rep. NSC86-2211-E032-007*, National Science Council, Taiwan, Republic of China (in Chinese).

Lee, Y. H., Lee, C. T., and Bair, J. H. (1998). Modified deflection ratio procedures for backcalculation of concrete pavements. *Airport facilities: Innovations for the Next Century; Proc., 25th Int. Air Transp. Conf.*, ASCE, M. T. McNerney, eds., Austin, Texas, June 14-17, 480-495.

Lee, Y. H., and M. I. Darter (1994). "New Predictive Modeling Techniques for Pavements," *Transportation Research Record* 1449, National Research Council, pp. 234-245.

Lee, Y. H. and R. S. Sheu (2001). "Parameter Study of Load Transfer and Curling Effects on Rigid Pavement Deflections." CD-ROM, *Second International Symposium on Maintenance and Rehabilitation of Pavements and Technological Control,* July 29 - August 01, Auburn, Alabama.

Li, S., Fwa, T. F., and Tan, K. H. (1996). "Closed-form backcalculation of rigid-pavement parameters." *J. of Transp. Engrg., ASCE, 122(1)*, 5-11.

Li, S., Fwa, T. F., and Tan, K. H. (1997). "Back-calculation of parameters for slab on two-layer foundation system." *J. of Transp. Engrg., ASCE, 123(6)*, 484-488.

Li, S., Fwa, T. F., and Tan, K. H. (1998). "Parameters back-calculation for concrete pavement with two slab layers." *J. of Transp. Engrg., ASCE, 124(6)*, 567-572.

Microsoft (1998). *Microsoft Visual Basic (Ver. 6.0) Programmer's Guide and Language Reference*. Microsoft Taiwan Corp.

Thompson, M. R., G. Navneet (1999). *Wheel Load Interaction: Critical Airport Pavement Responses*. FAA, DOT95-C-001, Final Report.

Wu, H.-T. (2003). *Parameter Analysis and Verification for Jointed Concrete Pavements*. M.S. Thesis, Tamkang University, Tamsui, Taiwan, January 2003. (In Chinese)